Molecular structure and environment dependence of shear-driven chemical reactions: Tribopolymerization of methylcyclopentane, cyclohexane and cyclohexene on stainless steel

Seong H Kim (shk10@psu.edu)
The Pennsylvania State University
Yu-Sheng Li
The Pennsylvania State University
Seokhoon Jang
The Pennsylvania State University
Fakhrul Hasan Bhuiyan
University of California Merced
Ashlie Martini
University of California Merced

Research Article

Keywords:

Posted Date: October 10th, 2022

DOI: https://doi.org/10.21203/rs.3.rs-2114274/v1

Abstract

Tribochemistry, which is another name of mechanochemistry driven by shear, deals with complex and dynamic interfacial processes that can lead to facilitation of surface wear or formation of beneficial tribofilms. For better mechanistic understanding, we investigated the reactivity of tribopolymerization of organic molecules with different internal ring strain energy (methylcyclopentane, cyclohexane, and cyclohexene) on a stainless steel (SS) surface in inert (N_2), oxidizing (O_2), and reducing (H_2) environments. On the clean SS surface, precursor molecules were found to physisorb with a broad range of molecular orientations. In inert and reducing environments, the strain-free cyclohexane showed the lowest tribochemical activity among the three tested. Compared to the N_2 environment, the tribochemical activity in H_2 was suppressed. In the O_2 environment, only cyclohexene produced tribofilms and methylcyclopentane and cyclohexane did not. When tribofilms were analyzed with Raman spectroscopy, the spectral features of diamond-like carbon (DLC) or amorphous carbon (a-C) were observed due to photochemical degradation of triboproducts. Based on infrared spectroscopy, tribofilms were found to be organic polymers containing oxygenated groups. Whenever polymeric tribrofilms were produced, wear volume was suppressed by orders of magnitudes but not completely to zero. These results supported the previously suggested mechanisms which involved surface oxygens as a reactant species of the tribopolymerization process.

Introduction

Tribochemistry is the study of chemical reactions that are facilitated by friction at a sliding interface. Tribochemical reactions could result from frictional heat or the exposure of highly reactive sites and dangling bonds [1–5]. When frictional heating and surface wear are negligible, tribochemical reactions occur via direct mechanical activation of interfacial molecules or atomic sites in the sliding interface [6–8]. It has been shown that tribofilms formed from tribochemical reactions of lubricant additives prevent the direct contact of asperities on the mating surfaces, hence minimizing friction and wear [9–12]. The prototypical film forming material is zinc dithiophosphate (ZDDP), a widely-used anti-wear additive that decomposes upon frictional shear to form a tribofilm that can protect surfaces and reduce wear [13–15]. However, thermal decomposition products of ZDDP in internal combustion engines of automobile can deteriorate the performance of the catalytic converter in the exhaust line [10, 16]. Thus, developing alternative anti-wear additives is imperative, but this requires better understanding of tribochemical reaction pathways and the mechanisms that lead to the formation of functional tribofilms.

Shear-induced tribofilm formation can vary depending on applied stress, molecular structure of reactants, environmental gas, and surface chemistry of materials involved [13, 17–21]. Numerous tribochemistry investigations have demonstrated an exponential relationship between applied stress or mechanical force and reaction rate or yield [13, 22–26]. For example, the growth of tribopolymer from α-pinene on dehydroxylated silica in N_2 was found to have an exponential relationship with applied stress [23]. In a study of wear reduction by cyclopropylcarboxylic acid (CPCa), which has a highly strained three-

membered ring, the zero-stress activation energy was found to be comparable to the C-C bond dissociation energy within cyclopropane, indicating that opening of the 3-membered ring was involved in tribochemical activation [27, 28]. In the tribochemical polymerization study of α-pinene, pinane, and n-decane, the tribochemical activity was found to be the highest for α-pinene which has the highest ring strain due to the presence of the 4-membered ring and a double bond in the 6-membered ring [11]. Reactive molecular dynamics (MD) simulations showed that the double bond in the ring can provide a reaction path that is not accessible in thermal reaction conditions [29]. This computational study also suggested that the structural deformation of reacting species by shear may contribute to the mechanical activation of tribochemical reactions [29].

In addition to quantifying the tribochemical reactivity of organic molecules, it is also important to chemically characterize the produced tribofilms. In the literature, Raman spectroscopy has been extensively employed to analyze tribofilms formed from organic precursors [14, 28, 30–36]. Vibrational spectral features reported for such tribofilms often showed two broad bands at ~ 1370 cm^{-1} and ~ 1580 cm^{-1}, which are very similar to characteristic bands of amorphous carbon (a-C) or diamond-like-carbon (DLC) materials [14, 28, 30–36]. Since these carbon materials are well known to reduce friction and wear, their formation could explain the good lubrication efficiency with substantial wear reduction in tribochemistry studies of organic precursors [30, 36, 37]. However, it should be noted that a-C and DLC are usually produced by high-energy physical or chemical vapor deposition processes or pyrolysis at extremely high temperatures [38, 39]. Thus, their formation must be tested and confirmed (or disputed) via independent analysis [40]. For a better understanding of tribochemical mechanism, having knowledge of the chemical nature of tribofilms is critical.

In this work, we studied the molecular structure dependence of tribopolymerization reactions of adsorbed organic precursors and demonstrated several methods for characterizing the tribofilm products. Vapor phase lubrication (VPL) has been demonstrated to effectively minimize friction and wear of various inorganic surfaces [16, 37, 41–47]. In VPL, lubricating molecules are delivered to the sliding interface via adsorption from the gas phase. Since there is no liquid solvent, tribochemical reaction products with vapor pressure lower than the delivered precursor molecule will remain on the surface, which allows further characterization of triboproducts [2, 4, 22, 48–50]. Here, methylcyclopentane (CH_3-c-C_5H_9), cyclohexane (c-C_6H_{12}), and cyclohexene (c-C_6H_{10}) were chosen to evaluate the reactivities of cyclic compounds with a 5-membered ring versus a 6-membered ring, as well as the impact of C = C double bond in the 6-membered ring. The ring strain is smaller in the cyclohexane than the cyclopentane [51]. In addition to precursor molecular structures, the effect of surrounding gas – inert (dry N_2), reducing (10% H_2 in N_2), and oxidizing (O_2) environment – was also evaluated. To investigate the interaction between organic vapors and the surface, polarization-modulation reflection absorption infrared spectroscopy (PM-RAIRS) and MD simulations were used to measure the adsorption isotherms and geometry, respectively, of cyclic hydrocarbons on stainless steel surfaces at ambient temperature. The produced tribofilms were analyzed with energy-dispersive X-ray (EDX) mapping for elemental composition, as well as Raman and infrared spectroscopy for chemical structures.

Methods

Experimental Methods

A bidirectional ball-on-flat tribometer was used to study tribochemical reactions of methylcyclopentane (97%; Sigma-Aldrich), cyclohexane (≥ 99%; Sigma-Aldrich) and cyclohexene (99%; Thermo Scientific) in dry N_2 (moisture volume concentration ~ 18 ppm), dry O_2 (purity 99.994%) and dry H_2 (10% in N_2) gas environments. The bearing-grade ball (diameter = 3mm) and substrate were AISI 440C stainless steel (SS; McMaster-Carr). The substrate was polished to RMS roughness of roughly 20 nm using various grits of sandpaper and a 0.03 μm alumina colloidal solution. The RMS roughness of the ball was ~ 6 nm [52]. The substrate and ball were both rinsed with ethanol followed by water and UV/Ozone for 30 minutes prior to tribo-testing [47]. The applied normal load was kept at 0.5 N. At this load the maximum Hertzian contact pressure was calculated to be ~ 0.45 GPa. The sliding speed was kept at 3 mm/s, so the average increase of flash temperature was less than 5°C [11, 17]. The length of the sliding track was 2.4 mm. The saturated vapor stream of each precursor was produced by flowing dry N_2, dry O_2 or dry H_2 (10% in N_2) into a flask containing the corresponding liquid, and a target partial pressure relative to its saturation (P/P_{sat}) was obtained by mixing the vapor-free gas stream with the saturated vapor stream at the corresponding ratio [25, 52]. The adsorption isotherms of organic vapor on polished stainless steel (SS) surface were studied with PM-RAIRS. For PM-RAIRS experiment, a ThermoNicolet Nexus 670 spectrometer equipped with an MCT detector and a Hinds Instrument photoelastic modulator was used. The modulator generated the P- and S-polarizations, alternating at 50 kHz of the incident IR beam. The P-polarization has the electric field parallel to the incidence beam plane, while the S-polarization has the field perpendicular to the plane [53, 54]. The P + S sum signal gives the vibrational spectrum of mostly gaseous species, while the (P-S)/(P + S) signal, difference normalized with total signal, solely provides the vibrational spectrum of the adsorbed species [53, 55]. The spectral resolution was set at 4 cm^{-1} for the SS experiment. For comparison, another PM-RAIRS measurement was done for a gold (Au) surface with a 1 cm^{-1} resolution. All spectra shown in this study were normalized with the spectrum collected with a clean surface in dry N_2 or O_2 spectrum as the background.

Tribofilms accumulated on the sliding track were imaged with atomic force microscopy (AFM; Digital instrument, Multimode). The imaging was done in tapping-mode with Bruker TESPA-V2 probes. Tribopolymerization yield was then estimated by calculated the volume above the reference plane, which was the pristine SS substrate surface outside the sliding track [11]. 3D optical profilometry (Zygo NewView 7300) was used to image the topography of the sliding track to estimate the wear volume after solvent-rinsing of triofilms produced and accumulated from 600 reciprocating cycles of sliding.

A Bruker Hyperion 3000 IR Microscope coupled to an IFS 66/s spectrometer was used for IR analysis. A reflective objective lens 15· (NA = 0.4) was used to analyze an area of 50·50 $μm^2$. The IR spectra were collected with 4 cm^{-1} resolution and averaged over 400 scans. For Raman analysis, a Horiba LabRam HR Evolution Vis-NIR system with an objective lens 100· (NA = 0.9) was used. In Raman data collection, the

acquisition time was 1s and the data were accumulated 10 times. Elemental analysis of the tribofilm via energy-dispersive x-ray (EDX) mapping was carried out using an Apreo S system (Thermo Fisher Scientific) with an electron accelerating voltage of 15kV.

Computational Methods

Molecular dynamics (MD) simulation was used to study the adsorption of cyclohexane, cyclohexene, and methylcyclopentane on amorphous Fe_2O_3 and Fe_3O_4 surfaces. Instead of chromium oxide covering the SS surface, iron oxides were used in the simulation due to the lack appropriate force field to simulation reactions on chromium oxide and the availability of force fields for Fe_2O_3 and Fe_3O_4 [56–59]. Two model systems were designed using QuantumATK [60], one for monolayer coverage and the other for sub-monolayer coverage on the iron oxide. The model for monolayer coverage contained 100 molecules of one of the three precursors, while the system for sub-monolayer coverage contained 30 molecules.

The amorphous iron oxide slabs were created using a heat and quench method that involved heating a crystalline Fe_2O_3 or Fe_3O_4 slab to 4000 K and then cooling it back to room temperature. Next, a vacuum region was inserted on top of the slabs to create surfaces. The amorphous surfaces were then passivated through reactions with water molecules until the number of reactions between the water and the surface reached steady state. The final dimensions of the amorphous slabs were 5 nm × 5 nm × 1.3 nm (length × width × thickness). The positions of atoms at the bottommost 0.4 nm of each slab were fixed. The organic molecules were placed randomly about 1 nm above the surface.

The simulation process started with energy minimization, followed by dynamic simulations of thermal equilibration at 300 K. Then the system temperature was increased to 450 K at 0.1 K/ps heating rate. This heating rate has been used previously to capture the adsorption process of tricresyl phosphate [61]. A repulsive wall was placed at the top of the simulation box to prevent atoms from leaving the simulation box. The canonical ensemble (NVT) was applied to all unconstrained atoms and charge equilibration was performed throughout the simulation. The initial simulation box dimensions were 5 × 5 × 6 nm^3 with periodic boundary conditions along the surface and fixed boundaries in the surface-normal direction.

The interactions between atoms were modeled using the ReaxFF force field [62, 63] with a set of parameters previously developed for Fe/P/O/C/H [64]. This force field has previously been used to simulate phosphorus-containing organic molecules on Fe, Fe_2O_3, and Fe_3O_4, where the adsorption and dissociation energies were reproduced accurately [59, 61, 64]. The time step for dynamics was 0.25 fs. All simulations were performed using the Large Atomic/Molecular Massively Parallel Simulation (LAMMPS) software [65]. Postprocessing was carried out using in-house python scripts and OVITO software [66].

Results And Discussion

Adsorption of precursors on SS surface in VPL condition

First, it is important to know how precursor molecules supplied through the vapor phase are adsorbed on the substrate surface. For that purpose, PM-RAIRS analysis was performed since this technique could selectively detect the vibrational spectrum of molecular species adsorbed on metal surfaces that are in equilibrium with the same molecules in the gas phase [54]. Figure 1 shows the PM-RAIRS spectra of methylcyclopentane, cyclohexane, and cyclohexene adsorbed on the SS surface. For comparison, the vapor phase spectra of the precursors are also plotted in Fig. 1.

In Fig. 1a, the gas phase spectrum of methylcyclopentane shows both symmetric and antisymmetric stretch modes of the CH_3 group at 2878 cm^{-1} and 2962 cm^{-1}, respectively, along with broad side bands or shoulders due to rovibrational excitations [67]. In contrast, the PM-RAIRS spectra of the methylcyclopentane adsorbed on the SS surface show only one sharp peak at 2962 cm^{-1}, which is the asymmetric stretch (v_a) mode of CH_3, and the symmetric stretch (v_s) peak of CH_3 is negligible at 2878 cm^{-1}. The same trend was observed in the higher-resolution PM-RAIRS spectra of methylcyclopentane adsorbed on the Au surface (Figure S1). On metallic surfaces with free electrons in the conduction band, only the surface-normal component can be detected in PM-RAIRS and the vibrational mode parallel to the surface is not detected due to the screening by the image charge in the substrate [68]. Thus, the absence of the CH_3 symmetric stretch peak means that the CH_3 side group of methylcyclopentane is parallel to the surface. In the PM-RAIRS spectra of the methylcyclopentane adsorbed on SS, side band tails with small intensities due to rovibrational broadening are still noticeable around the CH_3 asymmetric stretch peak. The CH_2 asymmetric vibration peak is not observed at ~ 2935 cm^{-1}, because its IR absorption cross-section is small (so its intensity is much smaller than the CH_3 asymmetric peak in the vapor phase spectrum).

In the PM-RAIRS spectra of cyclohexane adsorbed on the SS surface shown in Fig. 1b (and on Au in Figure S1 as well), the CH_2 asymmetric peak (v_a) is very strong at 2935 cm^{-1}. The CH_2 symmetric peak (v_s) of the adsorbate spectrum is negligible at 2860 cm^{-1}, while it is quite strong in the gas phase spectrum (again with the broad rovibrational bands in both side of the peak). In the case of cyclohexene (Fig. 1c), the stretch mode of the sp^2 C-H group can be seen at ~ 3040 cm^{-1} in the vapor phase spectrum, but this peak is negligible in the PM-RAIRS spectrum. This means that the C = C double-bond of cyclohexene is parallel to the surface. Similar to the methylcyclopentane case, the weak rovibrational side bands are evident around the CH_2 asymmetric stretch peak in the PM-RAIRS of cyclohexane and cyclohexene adsorbed on the SS surface.

In Fig. 2, the peak areas of the PM-RAIRS spectra are plotted as a function of relative partial pressure (P/P_{sat}) of each precursor molecule in the gas phase. The PM-RAIRS peak area is proportional to the surface coverage; thus, this plot is effectively equivalent to the adsorption isotherm [69]. The maximum P/P_{sat} employed in this study was 50%; beyond this, the vapor phase signal of the PM-RAIRS measurement was saturated. In this P/P_{sat} range, the adsorbate signal intensity (peak area) increases nonlinearly with a concave curvature [70–72]. This is characteristic of a type-III adsorption isotherm,

which is observed when the adsorbate-substrate interaction is weaker than the adsorbate-adsorbate interaction [70, 73]. When the precursor vapor was purged out, the PM-RAIRS signal decreased to the initial baseline, indicating that there was no residue or chemisorbed species on the SS substrate surface. In other words, the SS surface was inert, i.e., did not react with the precursor molecules studied here at room temperature. All molecules were physisorbed in the absence of associated shear force, suggesting that the interaction between cyclic hydrocarbon and SS is primarily governed by Van der Waals force; thus, any species remaining on the surface after frictional shear must be formed via tribochemical reactions.

To better understand the molecular adsorption geometry, reactive MD simulations were carried out simulating the adsorption process of the three precursor molecules on iron oxide surfaces. No chemisorption of the molecules was observed on stoichiometric hematite (Fe_2O_3) and magnetite (Fe_3O_4) surfaces in the reactive simulations; only molecular physisorption occurred. The orientation of the physisorbed molecules were investigated by analyzing the ring plane tilt angle of those molecules with respect to the surface. Further, the positions of the C1-C6 side chain of methylcyclopentane and C1 = C2 double bond of cyclohexene were characterized by analyzing the angle they made with the substrate surface. The trends observed in the results for monolayer coverage on Fe_2O_3 and Fe_3O_4, shown in Figure S2, were similar to the trends observed in the results for simulations with Fe_2O_3 surface in sub-monolayer coverage, which is shown in Fig. 3.

In all simulations, the orientation angle distributions of the C1-C6 side group of methylcyclopentane and the C1 = C2 double bond of cyclohexene (Fig. 3, Figure S2, orange bars) are centered around 0° and 180°, which is consistent with the experimental finding from the PM-RAIRS analysis (Fig. 1). The distributions for the ring plane tilt angles with respect to the surface in Fig. 3 and Figure S2 (black bars) averaged around 90°, suggesting that the precursor molecules adsorbed on oxide surfaces were tilted. This is somewhat different from the cryogenic temperature condition in which cyclic organic molecules typically adsorb with their molecular planes parallel to the surface [74]. All distributions reported in Fig. 3 and Figure S2 have standard deviations of at least 25°. Such broad distributions are probably consequences of dynamic interactions among adsorbates which are in equilibrium with the gas phase molecules at 300 K. This is because the interactions between adsorbates are stronger than interactions with the substrate, which is the characteristic of type-III adsorption isotherm.[70, 73] The dynamic equilibrium with the gas phase molecules may explain the presence of weak rovibrational features in the PM-RAIRS spectra of adsorbate species (Fig. 1) which are absent in the spectra of adsorbates on metal surfaces at cryogenic temperatures [75–77].

VPL efficiency and tribopolymerization yield

When the molecule of interest shows the type-II adsorption isotherm, the VPL study is typically carried out in the P/P_{sat} condition at which the formation of monolayer coverage is assured [69, 78]. However, due to the type-III adsorption isotherm (Fig. 2), it could not be determined the P/P_{sat} forming the monolayer coverage of precursors on the clean SS surface [69]. Nonetheless, it was empirically found that when

P/P_{sat} was 30% or above, all three precursors provided sufficient lubrication (Fig. 4b), as determined by the ability to suppress wear of the substrate in dry N_2 environment. When P/P_{sat} was 15%, there was noticeable wear of the SS substrate. Thus, all tribochemical measurements were conducted at P/P_{sat} = 30%. Since the adsorbate-adsorbate interaction is favored (as implied from the type-III adsorption isotherm), it was expected that once tribopolymerization was initiated, leaving a small amount of polymer in the sliding track, the precursor vapor would readily absorb into the polymer, facilitating further reactions in subsequent sliding cycles.

Figure 4a compares the coefficient of steady-state friction of the self-mated 440C SS surface in different vapor conditions. Figure 4b depicts the wear volume per reciprocating sliding cycle (i.e., wear rate) calculated after 600 bidirectional sliding at the applied contact stress of ~ 450 MPa. In the absence of precursor vapor, the coefficient of friction was around 0.7, and the surface exhibited severe wear [53, 69]. When significant wear occurred, the sliding track appeared dark in the optical image due to light scattering from the rough surface, and particulate debris were accumulated around the sliding track. In N_2 and H_2 environments, the presence of all three precursors tested at P/P_{sat} = 30% reduced the friction coefficient to approximately 0.23, which was close to a typical value reported for VPL of organic molecules [29, 78]. The friction coefficient gradually reached to a steady-state value within 50 cycles and was kept at the similar value until stopping the measurement at 600 cycles (Figure S3). The wear rate also decreased by about three orders of magnitude compared to the precursor-free environment (Fig. 4b). In addition, triboproducts with iridescent color could be seen in optical microscopy images, which is typical of polymeric tribofilms with varying thickness [11]. When O_2 was used as the carrier gas, methylcylcopentane and cyclohexane did not show any significant change in friction as compared to the precursor-free environments (Fig. 4a) and wear volumes were about two orders of magnitude higher than in N_2 and H_2 environments (Fig. 4b). Only cyclohexene could provide sufficient VPL along with formation of lubricious tribofilms that could be seen with optical microscopy.

Since the pristine SS surface was chemically inert in the absence of any frictional shear in the vapor environments tested (Figs. 1 and 2), the tribofilms can be attributed to the product of tribopolymerization of physisorbed molecules taking place upon frictional shear by the counter-surface. The tribopolymerization yield was determined by estimating the volume of the tribofilm above the reference plane using tapping-mode AFM. Figure 5a shows AFM images of the endpoints and middle of sliding tracks after tribopolymerization reactions of cyclohexene in N_2, O_2, and H_2 environments. The AFM images of tribofilms produced from the methylcyclopentane and cyclohexane precursors in N_2 and H_2 environments are shown in Figure S4.

Figure 5b compares the tribopolymerization yields at the same applied load, sliding speed, and sliding distance for different precursor molecules in inert (N_2), reducing (10% H_2 in N_2), and O_2 gas environments. In N_2, cyclohexane showed the lowest yield among the three precursors tested. In H_2, the overall yields decreased by ~ 50% as compared to the inert gas environment, but the relativity trend among three precursor molecules was the same as the N_2 case. In O_2, methylcyclopentane and

cyclohexane did not produce any measurable amount of tribopolymer, and only cyclohexene produced the tribopolymer. The tribopolymerization yield of cyclohexene in the O_2 environment was about ~ 50% higher than that in the N_2 environment.

Chemical analysis of tribopolymerization products

The ends of the sliding tracks, where tribopolymerization products were accumulated, were analyzed with EDX mapping. Figure 6 compares the elemental compositions determined from EDX mapping of the track ends after VPL testing of the three precursors for 600 reciprocating cycles in inert (N_2), reducing (10% H_2 in N_2), and oxidizing (O_2) environments. As a reference, the chemical composition of the 440C SS measured outside the sliding track is also shown [79]. In the absence of precursor vapors, EDX analysis revealed the uptake of a large amount of oxygen without an increase in carbon. This must be due to oxidation of wear debris formed during shearing [17, 50]. It is possible that the wear debris was oxidized by a trace amount of oxygen in the test environment during the tribotesting or by air during the sample transfer for ex-situ analysis.

In the cases of methylcyclopentane and cyclohexane in O_2, the chemical compositions detected with EDX are similar to the severe wear cases observed in the friction test without precursors. This is consistent with the inefficiency of VPL by these precursors in O_2, as shown in Fig. 4. In the cases where tribofilms were formed (Fig. 5) and friction and wear were greatly reduced (Fig. 4), EDX indicated the accumulation of carbon-containing species at the ends of sliding tracks. The iron and chromium signals in these regions are primarily from the substrate beneath the tribofilms, as the probe depth of EDX is larger than the tribofilm thickness (less than 2 μm; Fig. 5) [80, 81]. EDX also found the presence of oxygen in tribofilms formed by oxygen-free precursors in N_2 and H_2 environments. Tribochemical reaction pathways studied by ReaxFF-MD suggested that methylcyclopentane, cyclohexane and cyclohexene react with surface oxygen to form the final triboproducts [82]. Determining whether these oxygen species are due to wear debris or incorporated into the tribopolymers required molecular spectroscopy.

In the tribochemistry literature, Raman analysis has been frequently employed for vibrational spectroscopic analysis of tribofilms formed from organic precursors [9, 27, 30–32, 34–36, 83–86]. Many previous studies reported the formation of a-C or hydrogenated DLC due to frictional activation of organic precursors and hypothesized that these carbon films formed *in situ* are responsible for lubrication and wear prevention [9, 27, 34–36, 84, 86]. To compare with such previous reports, we performed micro-Raman analysis of the tribofilms (Fig. 7).

In the wear tracks formed in the absence of precursor molecules in the gas phase, the spectral features characteristic of hematite (Fe_2O_3) and magnetite (Fe_3O_4) were observed (Figure S6) [87, 88]. After VPL testing for methylcyclopentane and cyclohexane in O_2, the slide track also showed the same oxide bands, although the relative intensities of the peaks at 630 cm^{-1} and 1300 cm^{-1} were slightly different. These results confirmed that methylcylcopentane and cyclohexane could neither prevent the wear of SS surface (Fig. 4) nor produce tribopolymers (Fig. 5) in the O_2 environment.

As can be seen in Fig. 7, all tribofilms identified in with AFM (Fig. 5) exhibited Raman spectra with broad D-band and G-band characteristic of a-C or H-DLC. Although this might be viewed as 'consistent with previous literature', we concluded that the vibrational spectral features of a-C or H-DLC were due to photochemical degradation of tribopolymerization products based on the following control experiments. Details of control experiments conducted to dispute the hypothesis claiming the tribochemical synthesis of a-C or H-DLC are provided in the subsequent paper [40].

To obtain molecular spectral features without the photochemical artifact, tribopolymers produced from methylcyclopentane, cyclohexane, and cyclohexene in the N_2 environment were analyzed with IR spectroscopy coupled with microscopy. As shown in Fig. 8, all tribopolymers formed from these three precursors exhibited similar vibrational spectral features: broad bands at ~ 1450 cm^{-1} which can be attributed to CH_2 bending modes and two bands at 2880 cm^{-1} and 2920 cm^{-1} that could be ascribed to symmetric and asymmetric stretches of alkyl groups, respectively. There was no discernable peak at ~ 3030 cm^{1} in the IR spectrum of the tribopolymers formed from cyclohexene, indicating that the C = C double-bonds are all converted to single bonds or dissociated during the tribopolymerization process[29, 82]. All tribopolymers showed a strong peak at ~ 1700 cm^{-1} and a broad band spanning from 3100 cm^{-1} up to 3700 cm^{-1}, indicating that they have carbonyl (C = O) and hydroxyl (O-H) groups. The precursor molecules do not have any oxygenated functional groups. Thus, they must come from the substrate. In fact, previous tribochemistry studies of a-pinene and pinane have also reported that the tribopolymers contained oxygenated functional groups[11, 20, 29, 89, 90], and those groups must originate from the involvement of surface oxygen atoms in tribochemical reactions[22, 23, 29].

Molecular structure dependence and environmental effect of tribopolymerization

In inert gas environment (N_2), the tribopolymerization yield was lower for cyclohexane as compared to methylcyclopentane and cyclohexene (Fig. 5). It is known that, among cycloalkanes, cyclohexane with the 6-membered ring has the lowest ring strain [91]. Thus, our result is consistent with the hypothesis that the ring strain of a precursor plays a role in tribochemical activation [51]. Reactive MD simulations have shown that, prior to tribochemical reaction, reactants undergo some physical deformation deviating from their equilibrium conformation [22, 29]. It is conceivable that the molecules with higher internal strain energy would be more susceptible to such deformation.

In the reducing environment (H_2), the relative effect of molecular structure of precursors was similar to the trend found in the N_2 environment, but the overall yield was lower than the N_2 case (Fig. 5). Reactive MD simulations suggested that the initial tribochemical activation step of cycloalkane involves dehydrogenation reaction by the surface oxygen [82]. In the presence of H_2 in the surrounding gas, it is likely that such dehydrogenation reactions may be suppressed because, even if surface oxygens are activated by frictional shear, they could react with H_2 impinging from the gas phase, forming stable hydroxyl groups. Our previous study showed that fully hydroxylated silica surface is not highly reactive,

as compared to dehydroxylated surface, toward tribochemical reaction of another organic precursor (α-pinene) [23].

In the oxidative environment (O_2), all three molecules physisorb as readily as in N_2 (Figure S1), but only the tribochemical reactions of cyclohexene can be activated effectively. In the case of cyclohexene, the oxidative chemisorption can occur at shear-activated surface sites through the C = C double bond [29, 82]. Once the precursor molecule is chemisorbed, it can be associated with other molecules during sliding [24, 28, 69, 78, 82]. The fact that tribochemical reactions of cycloalkane are negligible in O_2 indicates that dehydrogenative chemisorption is suppressed or passivated if the reactive surface sites are reacted with O_2 impinging from the gas phase. Even if iron atoms are momentarily exposed at the worn surface, they are likely to be oxidized by O_2 impinging from the gas phase. Overall, the oxygen might compete with cycloalkane for reaction sites on SS and, thus, tribochemical reactions of cycloalkane may not occur readily [33, 50, 92–94].

Conclusion

The effects of molecular structure (methylcyclopentane, cyclohexane, and cyclohexene) and ambient gas (N_2, O_2, and H_2) on tribochemical reactivity on stainless steel were investigated. Under the experimental conditions in this study, it was found that the more strained molecules (methylcyclopentane and cyclohexene) exhibited higher reaction yield than the nearly-strain-free molecule (cyclohexane) in all environmental conditions. This supports the hypothesis that the internal ring strain of a molecule can impact tribochemical reactivity since reacting species with higher internal strain are more susceptible to shear-induced structural deformation deviating from thermodynamic equilibrium conformation. Moreover, tribochemical reactivities in reducing (H_2) and oxidizing (O_2) environments were different to that in an inert (N_2) environment. Hydrogen could impede dehydrogenative reactions of the cyclic hydrocarbons by surface O atoms, and thus the reactivities were suppressed in H_2 as compared to N_2. In an oxidizing environment, dehydrogenative chemisorption of methylcyclohexane and cyclohexane were impeded, thus preventing the formation of tribopolymers, and resulting in severe wear. In contrast, tribopolymerization of cyclohexene, which could be activated by the oxidative chemisorption of C = C, was facilitated in O_2. Vibrational spectroscopic analysis of tribofilms showed that they are polymeric species containing C = O and OH groups. The presence of oxygenated groups in the formed tribopolymers supported the previously suggested mechanisms which involved the surface oxygen in the intermediate step.

Declarations

Acknowledgement.

This work was supported by the National Science Foundation (Grant No. CMMI-2038494 and 2038499).

References

1. Hsu, S.M., Gates, R.S. Effect of materials on tribochemical reactions between hydrocarbons and surfaces. Journal of Physics D: Applied Physics **39**:3128 (2006) http://doi.org/10.1088/0022-3727/39/15/S02
2. Hanyaloglu, B., Graham, E. Vapor phase lubrication of ceramics. Lubrication engineering **50**:814-820 (1994)
3. Gates, R., Hsu, M., Klaus, E. Tribochemical mechanism of alumina with water. Tribology transactions **32**:357-363 (1989) http://doi.org/10.1080/10402008908981900
4. Graham, E., Klaus, E. Lubrication from the vapor phase at high temperatures. ASLE transactions **29**:229-234 (1986) http://doi.org/doi.org/10.1080/05698198608981682
5. Alpas, A., Hu, H., Zhang, J. Plastic deformation and damage accumulation below the worn surfaces. Wear **162**:188-195 (1993) http://doi.org/10.1016/0043-1648(93)90500-L
6. Spikes, H. Stress-augmented thermal activation: Tribology feels the force. Friction **6**:1-31 (2018) http://doi.org/10.1007/s40544-018-0201-2
7. Tysoe, W. On Stress-Induced Tribochemical Reaction Rates. Tribology Letters **65** (2017) http://doi.org/10.1007/s11249-017-0832-x
8. Martini, A., Eder, S.J., Dörr, N. Tribochemistry: a review of reactive molecular dynamics simulations. Lubricants **8**:44 (2020) http://doi.org/10.3390/lubricants8040044
9. Kabel, J., Edwards, T.E.J., Hain, C., Kochetkova, T., Parkison, D., Michler, J., et al. A novel fiber-fretting test for tribological characterization of the fiber/matrix interface. Composites Part B: Engineering **206** (2021) http://doi.org/10.1016/j.compositesb.2020.108535
10. Asay, D.B., Dugger, M.T., Kim, S.H. In-situ vapor-phase lubrication of MEMS. Tribology Letters **29**:67-74 (2008) http://doi.org/10.1007/s11249-007-9283-0
11. He, X., Barthel, A.J., Kim, S.H. Tribochemical synthesis of nano-lubricant films from adsorbed molecules at sliding solid interface: Tribo-polymers from α-pinene, pinane, and n-decane. Surface Science **648**:352-359 (2016) http://doi.org/10.1016/j.susc.2016.01.005
12. Strawhecker, K., Asay, D.B., McKinney, J., Kim, S.H. Reduction of adhesion and friction of silicon oxide surface in the presence of n-propanol vapor in the gas phase. Tribology Letters **19**:17-21 (2005) http://doi.org/10.1007/s11249-004-4261-2
13. Zhang, J., Spikes, H. On the Mechanism of ZDDP Antiwear Film Formation. Tribology Letters **63** (2016) http://doi.org/10.1007/s11249-016-0706-7
14. Ito, K., Martin, J., Minfray, C., Kato, K. Formation mechanism of a low friction ZDDP tribofilm on iron oxide. Tribology transactions **50**:211-216 (2007) http://doi.org/10.1080/10402000701271010
15. Spikes, H. The history and mechanisms of ZDDP. Tribology letters **17**:469-489 (2004) http://doi.org/10.1023/B:TRIL.0000044495.26882.b5
16. Dörr, N., Agocs, A., Besser, C., Ristić, A., Frauscher, M. Engine oils in the field: A comprehensive chemical assessment of engine oil degradation in a passenger car. Tribology Letters **67**:1-21 (2019) http://doi.org/10.1007/s11249-019-1182-7

17. Barthel, A.J., Combs, D.R., Kim, S.H. Synthesis of polymeric lubricating films directly at the sliding interface via mechanochemical reactions of allyl alcohols adsorbed from the vapor phase. RSC Adv **4**:26081-26086 (2014) http://doi.org/10.1039/c4ra02283a
18. Felts, J.R., Oyer, A.J., Hernandez, S.C., Whitener, K.E., Jr., Robinson, J.T., Walton, S.G., et al. Direct mechanochemical cleavage of functional groups from graphene. Nat Commun **6**:6467 (2015) http://doi.org/10.1038/ncomms7467
19. Akchurin, A., Bosman, R. A Deterministic Stress-Activated Model for Tribo-Film Growth and Wear Simulation. Tribology Letters **65** (2017) http://doi.org/10.1007/s11249-017-0842-8
20. He, X., Pollock, A., Kim, S.H. Effect of Gas Environment on Mechanochemical Reaction: A Model Study with Tribo-Polymerization of α-Pinene in Inert, Oxidative, and Reductive Gases. Tribology Letters **67** (2019) http://doi.org/10.1007/s11249-019-1136-0
21. Rana, R., Bavisotto, R., Hou, K., Tysoe, W.T. Surface chemistry at the solid–solid interface: mechanically induced reaction pathways of C 8 carboxylic acid monolayers on copper. Physical Chemistry Chemical Physics **23**:17803-17812 (2021) http://doi.org/10.1039/d1cp03170h
22. Yeon, J., He, X., Martini, A., Kim, S.H. Mechanochemistry at Solid Surfaces: Polymerization of Adsorbed Molecules by Mechanical Shear at Tribological Interfaces. ACS Appl Mater Interfaces **9**:3142-3148 (2017) http://doi.org/10.1021/acsami.6b14159
23. Khajeh, A., He, X., Yeon, J., Kim, S.H., Martini, A. Mechanochemical Association Reaction of Interfacial Molecules Driven by Shear. Langmuir **34**:5971-5977 (2018) http://doi.org/10.1021/acs.langmuir.8b00315
24. Jacobs, T.D., Carpick, R.W. Nanoscale wear as a stress-assisted chemical reaction. Nat Nanotechnol **8**:108-112 (2013) http://doi.org/10.1038/nnano.2012.255
25. Martini, A., Kim, S.H. Activation Volume in Shear-Driven Chemical Reactions. Tribology Letters **69** (2021) http://doi.org/10.1007/s11249-021-01522-x
26. Gosvami, N., O'Shea, S. Nanoscale trapping and squeeze-out of confined alkane monolayers. Langmuir **31**:12960-12967 (2015) http://doi.org/10.1021/acs.langmuir.5b03133
27. Johnson, B., Wu, H., Desanker, M., Pickens, D., Chung, Y.-W., Jane Wang, Q. Direct Formation of Lubricious and Wear-Protective Carbon Films from Phosphorus- and Sulfur-Free Oil-Soluble Additives. Tribology Letters **66** (2017) http://doi.org/10.1007/s11249-017-0945-2
28. Khan, A.M., Wu, H., Ma, Q., Chung, Y.-W., Wang, Q.J. Relating Tribological Performance and Tribofilm Formation to the Adsorption Strength of Surface-Active Precursors. Tribology Letters **68** (2019) http://doi.org/10.1007/s11249-019-1249-5
29. Bhuiyan, F.H., Kim, S.H., Martini, A. Reactive molecular dynamics simulations of thermal and shear-driven oligomerization. Applied Surface Science **591** (2022) http://doi.org/10.1016/j.apsusc.2022.153209
30. Wu, H., Khan, A.M., Johnson, B., Sasikumar, K., Chung, Y.W., Wang, Q.J. Formation and Nature of Carbon-Containing Tribofilms. ACS Appl Mater Interfaces **11**:16139-16146 (2019) http://doi.org/10.1021/acsami.8b22496

31. Hesketh, J., Ward, M., Dowson, D., Neville, A. The composition of tribofilms produced on metal-on-metal hip bearings. Biomaterials **35**:2113-2119 (2014) http://doi.org/10.1016/j.biomaterials.2013.11.065
32. Khaemba, D.N., Neville, A., Morina, A. A methodology for Raman characterisation of MoDTC tribofilms and its application in investigating the influence of surface chemistry on friction performance of MoDTC lubricants. Tribology Letters **59**:1-17 (2015) http://doi.org/10.1007/s11249-015-0566-6
33. Zhang, J., Campen, S., Wong, J., Spikes, H. Oxidational wear in lubricated contacts–Or is it? Tribology International **165**:107287 (2022) http://doi.org/10.1016/j.triboint.2021.107287
34. Wimmer, M., Laurent, M., Mathew, M., Nagelli, C., Liao, Y., Marks, L., et al. The effect of contact load on CoCrMo wear and the formation and retention of tribofilms. Wear **332**:643-649 (2015) http://doi.org/10.1016/j.wear.2015.02.013
35. Liu, X., Yamaguchi, R., Umehara, N., Deng, X., Kousaka, H., Murashima, M. Clarification of high wear resistance mechanism of ta-CNx coating under poly alpha-olefin (PAO) lubrication. Tribology International **105**:193-200 (2017) http://doi.org/10.1016/j.triboint.2016.10.016
36. Erdemir, A., Ramirez, G., Eryilmaz, O.L., Narayanan, B., Liao, Y., Kamath, G., et al. Carbon-based tribofilms from lubricating oils. Nature **536**:67-71 (2016) http://doi.org/10.1038/nature18948
37. Jang, S., Chen, Z., Kim, S.H. Environmental effects on superlubricity of hydrogenated diamond-like carbon: Understanding tribochemical kinetics in O2 and H2O environments. Applied Surface Science **580**:152299 (2022) http://doi.org/10.1016/j.apsusc.2021.152299
38. Erdemir, A., Eryilmaz, O., Kim, S. Effect of tribochemistry on lubricity of DLC films in hydrogen. Surface and Coatings Technology **257**:241-246 (2014) http://doi.org/10.1016/j.surfcoat.2014.08.002
39. Devi, M., Rawat, S., Sharma, S. A comprehensive review of the pyrolysis process: From carbon nanomaterial synthesis to waste treatment. Oxford Open Materials Science **1**:itab014 (2021) http://doi.org/10.1093/oxfmat/itab014
40. Li, Y.-S., Jang, S., Khan, A.M., Martini, A., Wang, Q.J., Chung, Y.-W., et al. Tribofilm from organic precursor – Does DLC-like feature in Raman spectrum really mean it is DLC formed by friction? Tribology Letters (2022) (Submitted)
41. Kim, S.H., Asay, D.B., Dugger, M.T. Nanotribology and MEMS. Nano today **2**:22-29 (2007) http://doi.org/10.1016/S1748-0132(07)70140-8
42. Timpe, S.J., Komvopoulos, K. An experimental study of sidewall adhesion in microelectromechanical systems. Journal of microelectromechanical systems **14**:1356-1363 (2005) http://doi.org/10.1109/JMEMS.2005.859076
43. Gellman, A.J. Vapor lubricant transport in MEMS devices. Tribology Letters **17**:455-461 (2004) http://doi.org/10.1023/B:TRIL.0000044493.73585.e3
44. Komvopoulos, K., Yan, W. Three-dimensional elastic-plastic fractal analysis of surface adhesion in microelectromechanical systems. Journal of Tribology-Transactions of the Asme 120:808-813

(1998) http://doi.org/10.1115/1.2833783

45. Kim, H.-J., Seo, K.-J., Kang, K.H., Kim, D.-E. Nano-lubrication: A review. International Journal of Precision Engineering and Manufacturing **17**:829-841 (2016) http://doi.org/10.1007/s12541-016-0102-0
46. Shao, Y., Jacobs, T.D.B., Jiang, Y., Turner, K.T., Carpick, R.W., Falk, M.L. Multibond Model of Single-Asperity Tribochemical Wear at the Nanoscale. ACS Appl Mater Interfaces **9**:35333-35340 (2017) http://doi.org/10.1021/acsami.7b08023
47. Barthel, A.J., Luo, J., Hwang, K.S., Lee, J.-Y., Kim, S.H. Boundary lubrication effect of organic residue left on surface after evaporation of organic cleaning solvent. Wear **350-351**:21-26 (2016) http://doi.org/10.1016/j.wear.2015.12.010
48. Ren, D., Gellman, A.J. Reaction mechanisms in organophosphate vapor phase lubrication of metal surfaces. Tribology international 34:353-365 (2001) http://doi.org/10.1016/S0301-679X(01)00025-1
49. Van Treuren, K., Barlow, D., Heiser, W., Wagner, M., Forster, N. Investigation of vapor-phase lubrication in a gas turbine engine. Journal of Engineering for Gas Turbines and Power **120**:257-262 (1998) http://doi.org/10.1115/1.2818113
50. Fein, R., Kreuz, K. Chemistry of boundary lubrication of steel by hydrocarbons. ASLE TRANSACTIONS **8**:29-38 (1965) http://doi.org/10.1080/05698196508972076
51. Agapito, F., Nunes, P.M., Costa Cabral, B.J., Borges dos Santos, R.M., Martinho Simoes, J.A. Energetic differences between the five-and six-membered ring hydrocarbons: strain energies in the parent and radical molecules. The Journal of Organic Chemistry **73**:6213-6223 (2008) http://doi.org/10.1021/jo800690m
52. Barthel, A.J., Gregory, M.D., Kim, S.H. Humidity Effects on Friction and Wear Between Dissimilar Metals. Tribology Letters **48**:305-313 (2012) http://doi.org/10.1007/s11249-012-0026-5
53. Barthel, A.J., Kim, S.H. Lubrication by physisorbed molecules in equilibrium with vapor at ambient condition: effects of molecular structure and substrate chemistry. Langmuir **30**:6469-6478 (2014) http://doi.org/10.1021/la501049z
54. Barner, B.J., Green, M.J., Saez, E.I., Corn, R.M. Polarization modulation Fourier transform infrared reflectance measurements of thin films and monolayers at metal surfaces utilizing real-time sampling electronics. Analytical Chemistry **63**:55-60 (1991) http://doi.org/10.1021/ac00001a010
55. Asay, D.B., Kim, S.H. Molar volume and adsorption isotherm dependence of capillary forces in nanoasperity contacts. Langmuir **23**:12174-12178 (2007) http://doi.org/10.1021/la701954k
56. Evans, R.D., More, K.L., Darragh, C.V., Nixon, H.P. Transmission electron microscopy of boundary-lubricated bearing surfaces. Part I: Mineral oil lubricant. Tribology Transactions **47**:430-439 (2004) http://doi.org/10.1080/05698190490463286
57. Parkinson, G.S. Iron oxide surfaces. Surface Science Reports **71**:272-365 (2016) http://doi.org/10.1016/j.surfrep.2016.02.001
58. Chia, C.-L., Avendaño, C., Siperstein, F.R., Filip, S. Liquid adsorption of organic compounds on hematite α-fe2o3 using reaxff. Langmuir **33**:11257-11263 (2017)

http://doi.org/10.1021/acs.langmuir.7b02374.s001

59. Ewen, J.P., Latorre, C.A., Gattinoni, C., Khajeh, A., Moore, J.D., Remias, J.E., et al. Substituent effects on the thermal decomposition of phosphate esters on ferrous surfaces. The Journal of Physical Chemistry C **124**:9852-9865 (2020) http://doi.org/10.1021/acs.jpcc.9b11787
60. Smidstrup, S., Markussen, T., Vancraeyveld, P., Wellendorff, J., Schneider, J., Gunst, T., et al. QuantumATK: an integrated platform of electronic and atomic-scale modelling tools. Journal of Physics: Condensed Matter **32**:015901 (2019) http://doi.org/10.1088/1361-648X/ab4007
61. Khajeh, A., Bhuiyan, F.H., Mogonye, J.-E., Pesce-Rodriguez, R.A., Berkebile, S., Martini, A. Thermal decomposition of tricresyl phosphate on ferrous surfaces. The Journal of Physical Chemistry C **125**:5076-5087 (2021) http://doi.org/10.1021/acs.jpcc.0c10789
62. Senftle, T.P., Hong, S., Islam, M.M., Kylasa, S.B., Zheng, Y., Shin, Y.K., et al. The ReaxFF reactive force-field: development, applications and future directions. npj Computational Materials **2**:1-14 (2016) http://doi.org/10.1038/npjcompumats.2015.11 10.1038/npjcompumats.2015.11
63. Chipara, A., Tsafack, T., Owuor, P., Yeon, J., Junkermeier, C., van Duin, A., et al. Underwater adhesive using solid–liquid polymer mixes. Materials today chemistry **9**:149-157 (2018) http://doi.org/10.1016/j.mtchem.2018.07.002
64. Khajeh, A., Hu, X., Mohammadtabar, K., Shin, Y.K., Van Duin, A.C., Berkebile, S., et al. Statistical analysis of tri-cresyl phosphate conversion on an iron oxide surface using reactive molecular dynamics simulations. The Journal of Physical Chemistry C **123**:12886-12893 (2019) http://doi.org/10.1021/acs.jpcc.9b02394
65. Plimpton, S. Fast parallel algorithms for short-range molecular dynamics. Journal of computational physics **117**:1-19 (1995) http://doi.org/10.1006/jcph.1995.1039
66. Stukowski, A. Visualization and analysis of atomistic simulation data with OVITO–the Open Visualization Tool. Modelling and simulation in materials science and engineering **18**:015012 (2009) http://doi.org/10.1088/0965-0393/18/1/015012
67. Bernath, P.F., Sibert III, E.L. Cyclohexane Vibrations: High-Resolution Spectra and Anharmonic Local Mode Calculations. The Journal of Physical Chemistry A **124**:9991-10000 (2020) http://doi.org/10.1021/acs.jpca.0c09185
68. Greenler, R.G., Snider, D., Witt, D., Sorbello, R. The metal-surface selection rule for infrared spectra of molecules adsorbed on small metal particles. Surface Science **118**:415-428 (1982) http://doi.org/10.1016/0039-6028(82)90197-2
69. He, X., Kim, S.H. Mechanochemistry of Physisorbed Molecules at Tribological Interfaces: Molecular Structure Dependence of Tribochemical Polymerization. Langmuir **33**:2717-2724 (2017) http://doi.org/10.1021/acs.langmuir.6b04028
70. Fagerlund, G. Determination of specific surface by the BET method. Matériaux et Construction **6**:239-245 (1973) http://doi.org/10.1007/BF02479039
71. Beaglehole, D., Christenson, H. Vapor adsorption on mica and silicon: entropy effects, layering, and surface forces. The Journal of Physical Chemistry **96**:3395-3403 (1992)

http://doi.org/10.1021/j100187a040

72. Wahida, F., Larese, J.Z. Adsorption of Cyclopentane on MgO(100), Hexagonal Boron Nitride, and Graphite Basal Planes: A Thermodynamic and Modeling Study. The Journal of Physical Chemistry C **122**:25301-25313 (2018) http://doi.org/10.1021/acs.jpcc.8b06487
73. Barthel, A.J., Al-Azizi, A., Surdyka, N.D., Kim, S.H. Effects of gas or vapor adsorption on adhesion, friction, and wear of solid interfaces. Langmuir **30**:2977-2992 (2014) http://doi.org/10.1021/la402856j
74. Saeys, M., Reyniers, M.-F., Neurock, M., Marin, G. Adsorption of cyclohexadiene, cyclohexene and cyclohexane on Pt (1 1 1). Surface science **600**:3121-3134 (2006) http://doi.org/10.1016/j.susc.2006.05.059
75. Cooper, E., Coats, A.M., Raval, R. Cyclohexane adsorption on clean and O-covered Ni {111}: implications for C—H bond activation. Journal of the Chemical Society, Faraday Transactions **91**:3703-3708 (1995) http://doi.org/10.1039/ft9959103703
76. Raval, R., Parker, S., Chesters, M. CH··· M interactions and orientational changes of cyclohexane on Cu (111): a RAIRS, EELS and LEED study. Surface science **289**:227-236 (1993) http://doi.org/10.1016/0039-6028(93)90655-4
77. Fosser, K.A., Nuzzo, R.G., Bagus, P.S., Wöll, C. The origin of soft vibrational modes of alkanes adsorbed on Cu: An experimental and theoretical investigation. The Journal of chemical physics **118**:5115-5131 (2003) http://doi.org/10.1063/1.1546266
78. Barthel, A.J., Al-Azizi, A., Surdyka, N.D., Kim, S.H. Effects of gas or vapor adsorption on adhesion, friction, and wear of solid interfaces. Langmuir **30**:2977-2992 (2014) http://doi.org/10.1021/la402856j
79. Yang, J., Yu, T., Wang, C. Martensitic transformations in AISI 440C stainless steel. Materials Science and Engineering: A **438**:276-280 (2006) http://doi.org/10.1016/j.msea.2006.02.098
80. Shojaei, T.R., Soltani, S., Derakhshani, M.: Synthesis, properties, and biomedical applications of inorganic bionanomaterials. Fundamentals of Bionanomaterials, pp. 139-174. Elsevier, Place Elsevier (2022)
81. Titus, D., Samuel, E.J.J., Roopan, S.M.: Nanoparticle characterization techniques. Green synthesis, characterization and applications of nanoparticles, pp. 303-319. Elsevier, Place Elsevier (2019)
82. Bhuiyan, F.H., Li, Y.-S., Kim, S. Shear-Activated Chemisorption and Association of Cyclic Organic Molecules. Faraday Discussions (2022) http://doi.org/10.1039/D2FD00086E
83. Adachi, K.: Superlubricity of carbon nitride coatings in inert gas environments. Superlubricity, pp. 189-214. Elsevier, Place Elsevier (2021)
84. Liao, Y., Pourzal, R., Wimmer, M., Jacobs, J., Fischer, A., Marks, L. Graphitic tribological layers in metal-on-metal hip replacements. Science **334**:1687-1690 (2011) http://doi.org/10.1126/science.1213902
85. Huynh, K.K., Tieu, K.A., Pham, S.T. Synergistic and Competitive Effects between Zinc Dialkyldithiophosphates and Modern Generation of Additives in Engine Oil. Lubricants **9**:35 (2021)

http://doi.org/10.3390/lubricants9040035

86. Argibay, N., Babuska, T., Curry, J., Dugger, M., Lu, P., Adams, D., et al. In-situ tribochemical formation of self-lubricating diamond-like carbon films. Carbon **138**:61-68 (2018) http://doi.org/10.1016/j.carbon.2018.06.006
87. Shebanova, O.N., Lazor, P. Raman study of magnetite (Fe3O4): laser-induced thermal effects and oxidation. Journal of Raman spectroscopy **34**:845-852 (2003) http://doi.org/10.1002/jrs.1056
88. Zoppi, A., Lofrumento, C., Castellucci, E., Sciau, P. Al-for-Fe substitution in hematite: the effect of low Al concentrations in the Raman spectrum of Fe2O3. Journal of Raman Spectroscopy: An International Journal for Original Work in all Aspects of Raman Spectroscopy, Including Higher Order Processes, and also Brillouin and Rayleigh Scattering **39**:40-46 (2008) http://doi.org/10.1002/jrs.1811
89. He, X., Ngo, D., Kim, S.H. Mechanochemical Reactions of Adsorbates at Tribological Interfaces: Tribopolymerizations of Allyl Alcohol Coadsorbed with Water on Silicon Oxide. Langmuir **35**:15451-15458 (2019) http://doi.org/10.1021/acs.langmuir.9b01663
90. He, X., Kim, S.H. Surface Chemistry Dependence of Mechanochemical Reaction of Adsorbed Molecules-An Experimental Study on Tribopolymerization of alpha-Pinene on Metal, Metal Oxide, and Carbon Surfaces. Langmuir **34**:2432-2440 (2018) http://doi.org/10.1021/acs.langmuir.7b03763
91. Anslyn, E.V., Dougherty, D.A.: Modern physical organic chemistry. University science books, (2006)
92. Roberts, R. Adsorption and decomposition of hydrocarbons on clean metal films. British Journal of Applied Physics **14**:485 (1963) http://doi.org/10.1088/0508-3443/14/8/308
93. Roberts, R.W. Reactions of Saturated Hydrocarbons with Clean Rhodium Films. Annals of the New York Academy of Sciences **101**:766-777 (1963) http://doi.org/10.1111/j.1749-6632.1963.tb54930.x
94. Gilroy, D., Mayne, J. The oxidation of iron at room temperature. Corrosion Science **5**:55-58 (1965) http://doi.org/10.1016/S0010-938X(65)90096-X

Figures

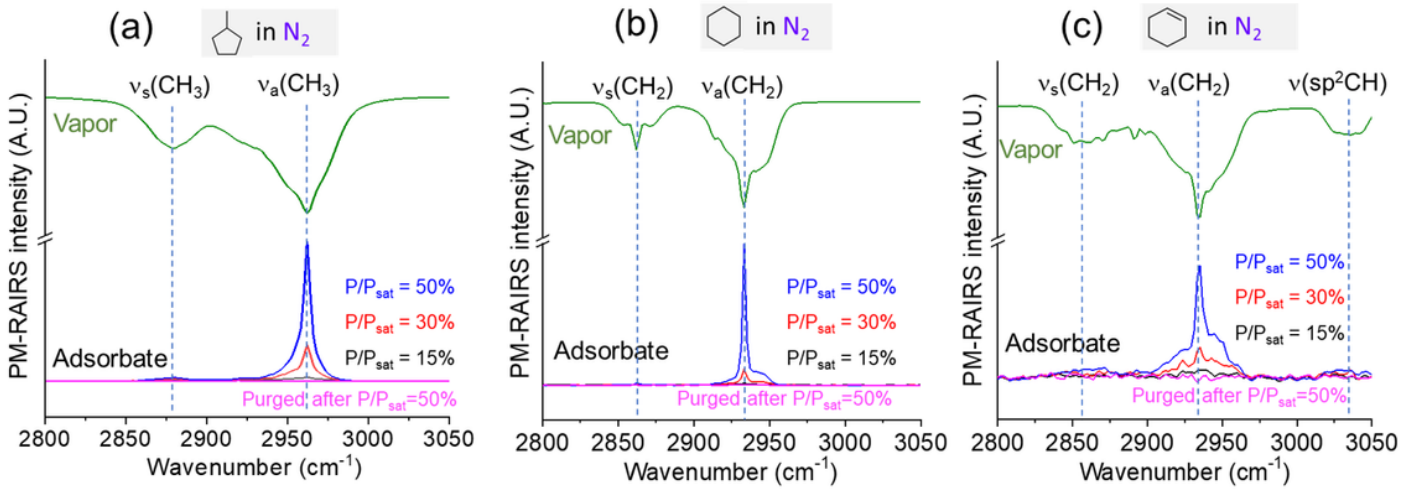

Figure 1

PM-RAIRS spectra of (a) methylcyclopentane, (b) cyclohexane, and (c) cyclohexene adsorbed on the stainless-steel surface at P/P_{sat} =15% (black), 30% (red), 50% (blue) and then after purging out organic vapor with N_2 (magenta). For comparison, the vapor phase spectrum of each precursor (green) is also shown. Above 50% P/P_{sat}, the vapor phase signal was saturated in our in-situ cell, so PM-RAIRS measurement could not be done. The PM-RAIRS spectra of the same precursors measured in O_2 as well as the PM-RAIRS spectra measured with a gold substrate are shown in Figure S1. (Color figure online)

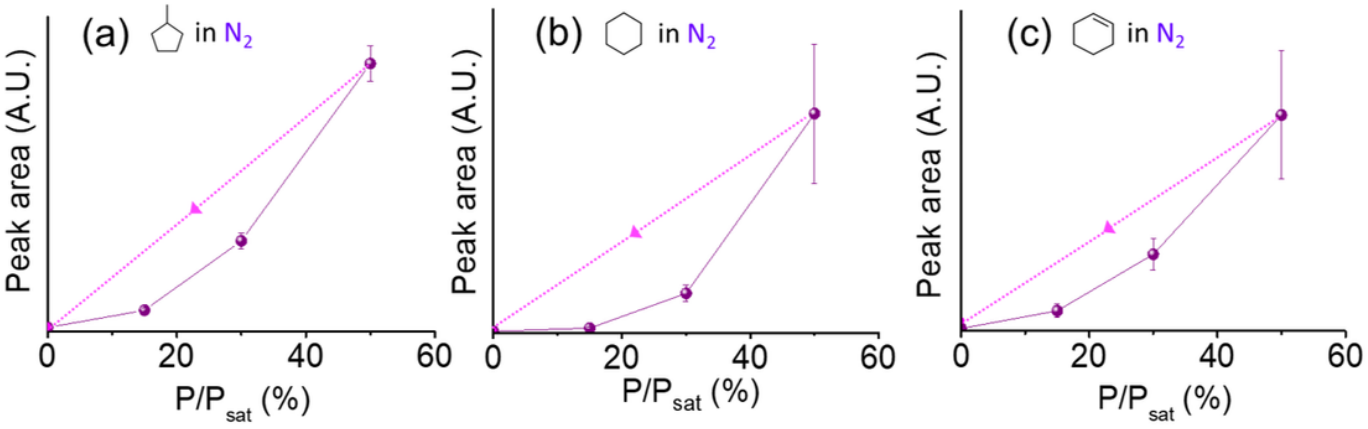

Figure 2

Peak areas of the C-H stretch modes of the adsorbate spectra of (a) methylcyclopentane, (b) cyclohexane, and (c) cyclohexene as a function of relative partial pressure (P/P_{sat}). The arrow (Magenta) indicates the data measured upon purging of the vapor after P/P_{sat}=50% measurement. Error bars are the standard deviation from three different measurements.

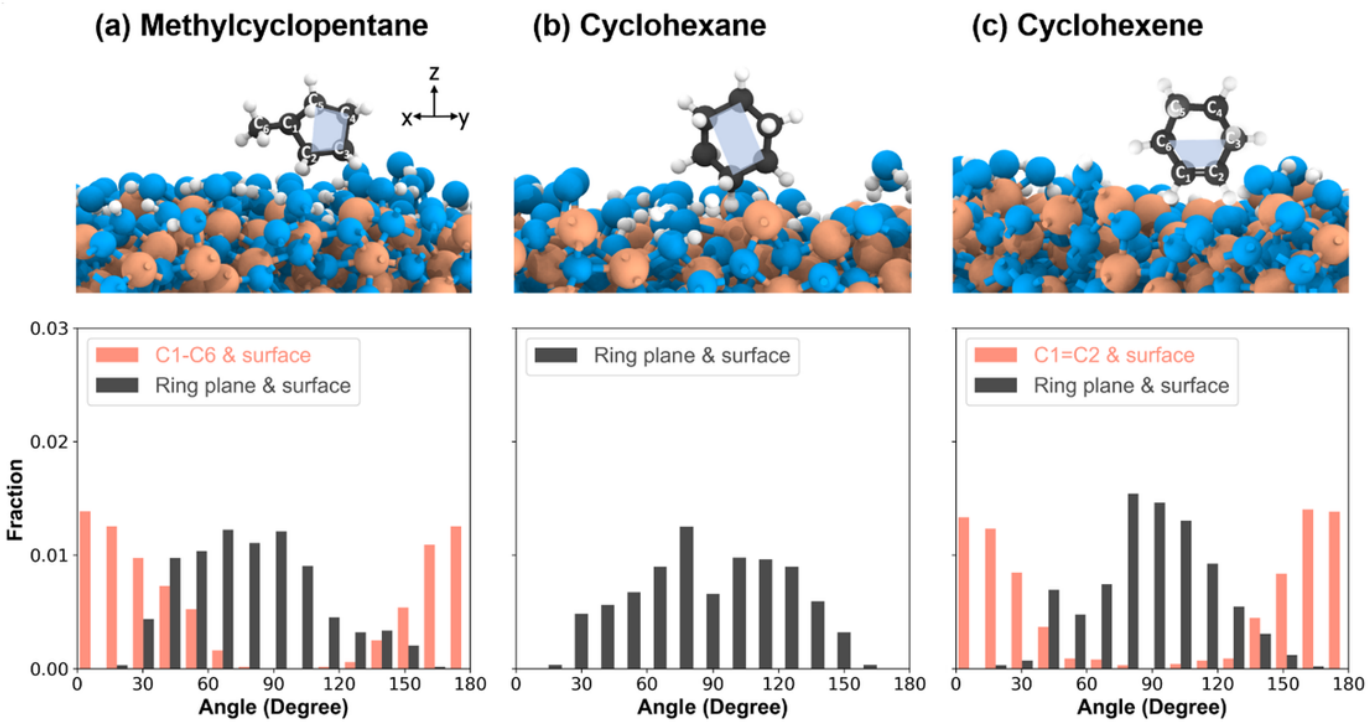

Figure 3

MD simulation results of (a) methylcyclopentane, (b) cyclohexane, and (c) cyclohexene on an amorphous Fe_2O_3 surface and sub-monolayer coverage. The upper row of the figure shows simulation snapshots of representative adsorbed molecules. The white, black, blue, and brown spheres represent H, C, O, and Fe atoms, respectively. The C atoms in methylcyclopentane and cyclohexene are numbered from 1 through 6 according to IUPAC convention. The blue trapezoid inside a molecule shows the four atoms used to define the plane of the ring. The black bars in the bottom row represent the distributions of the ring plane tilt angle, i.e., angle between the surface (XY plane) and the ring plane, while the orange bars represent the distributions of the angle between the surface and the C1-C6 methyl group side chain in (a), or C1=C2 double bond in (c).

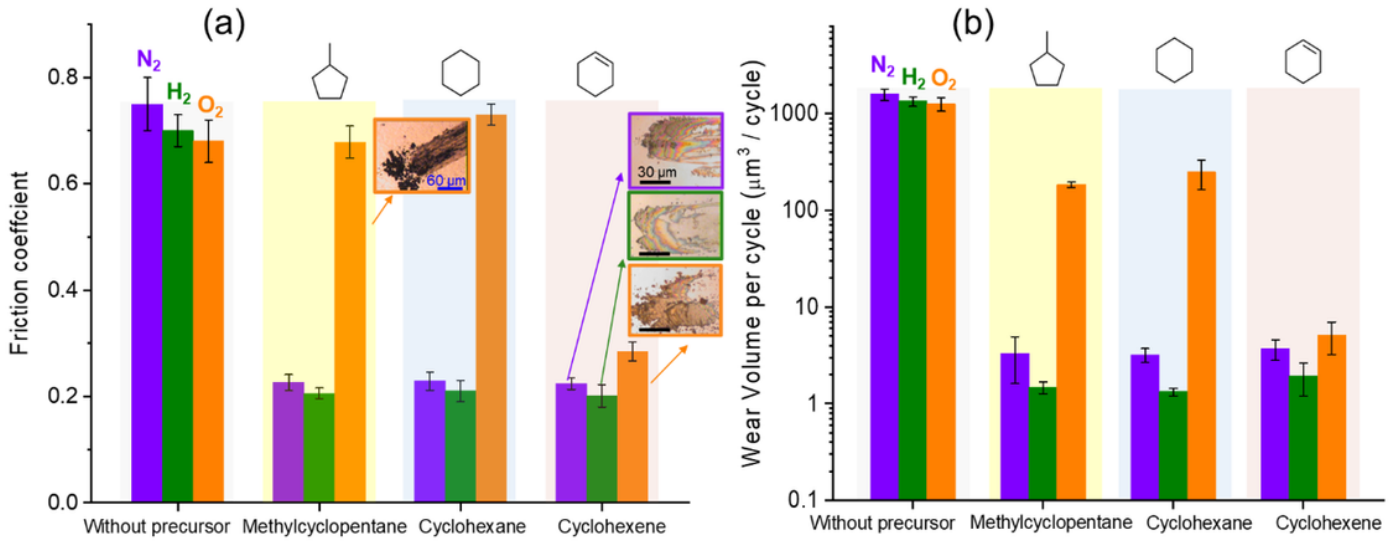

Figure 4

(a) Friction coefficient measured on SS in dry N_2, O_2, and H_2 without and with 30% P/P_{sat} of methylcyclopentane, cyclohexane, and cyclohexene. The error bars are standard deviations from more than five independent measurements. The optical microscope images show wear tracks formed in cyclohexane test in O_2, and triboproducts produced from cyclohexene and piled up at one end of the sliding track; images of other precursors are not shown. (b) Wear volume on the slide track measured with optical profilometry after 600 reciprocating cycles and removing triboproducts with acetone.

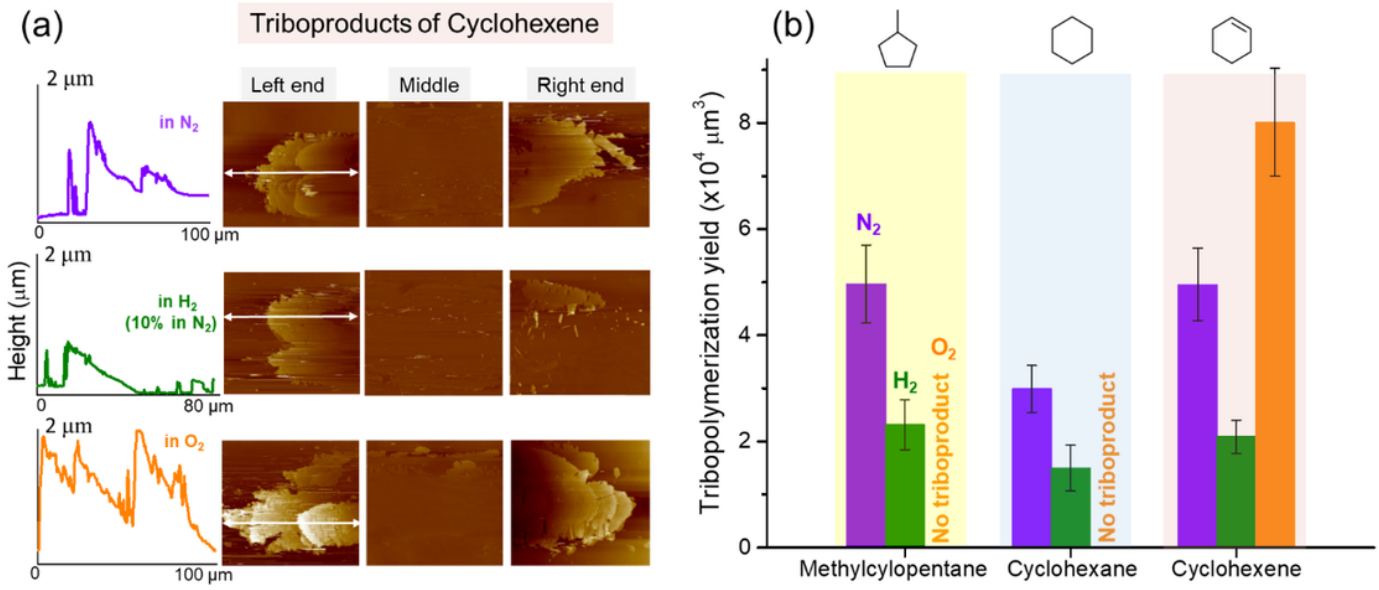

Figure 5

(a) AFM images (100 μm100 μm in N_2 and O_2 or 80 μm80 μm in H_2) of the left end, middle, and right end of the slide track after 600 reciprocating cycles of interfacial sliding in 30% P/P_{sat} cyclohexene in N_2, H_2, and O_2 environments. The height profiles of the products at the left ends are also shown. (b) Total amount of triboproducts was calculated by integrating the volume above the substrate surface plane. The error bars are standard deviations from three independent measurements.

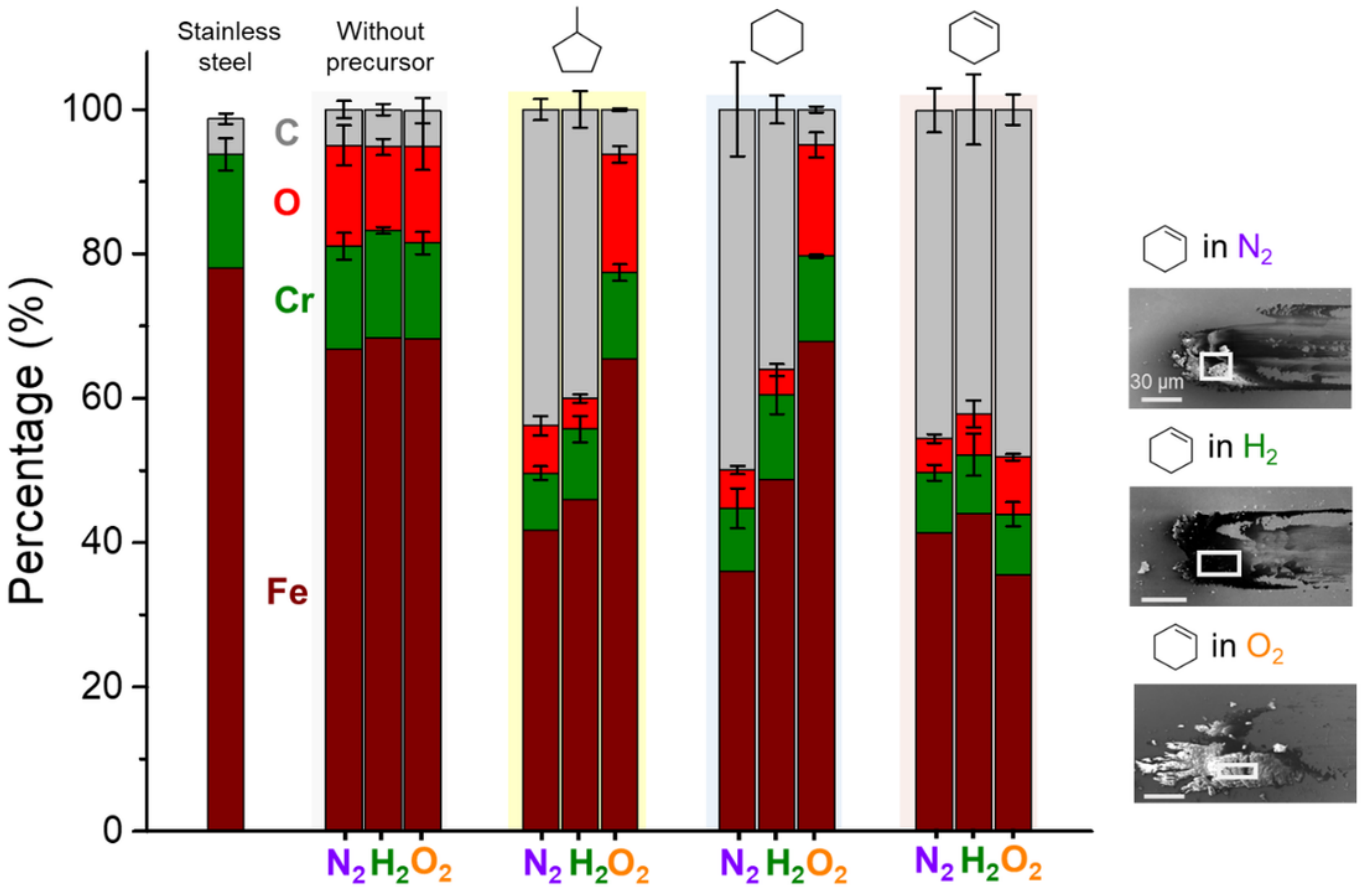

Figure 6

Elemental composition calculated from EDX mapping of the tribofilm region at the end of the sliding track formed after 600 reciprocating cycles in 30% P/P_{sat} of precursor vapors in inert (dry N_2), reducing (10% H_2 in N_2), and oxidizing (dry O_2) gas environments. The error bars are standard deviations from three different sliding tracks. Examples of analyzed areas are identified by white boxes in the SEM images shown in the right. More examples of EDX mapping at various locations for one sliding track are shown in Figure S5.

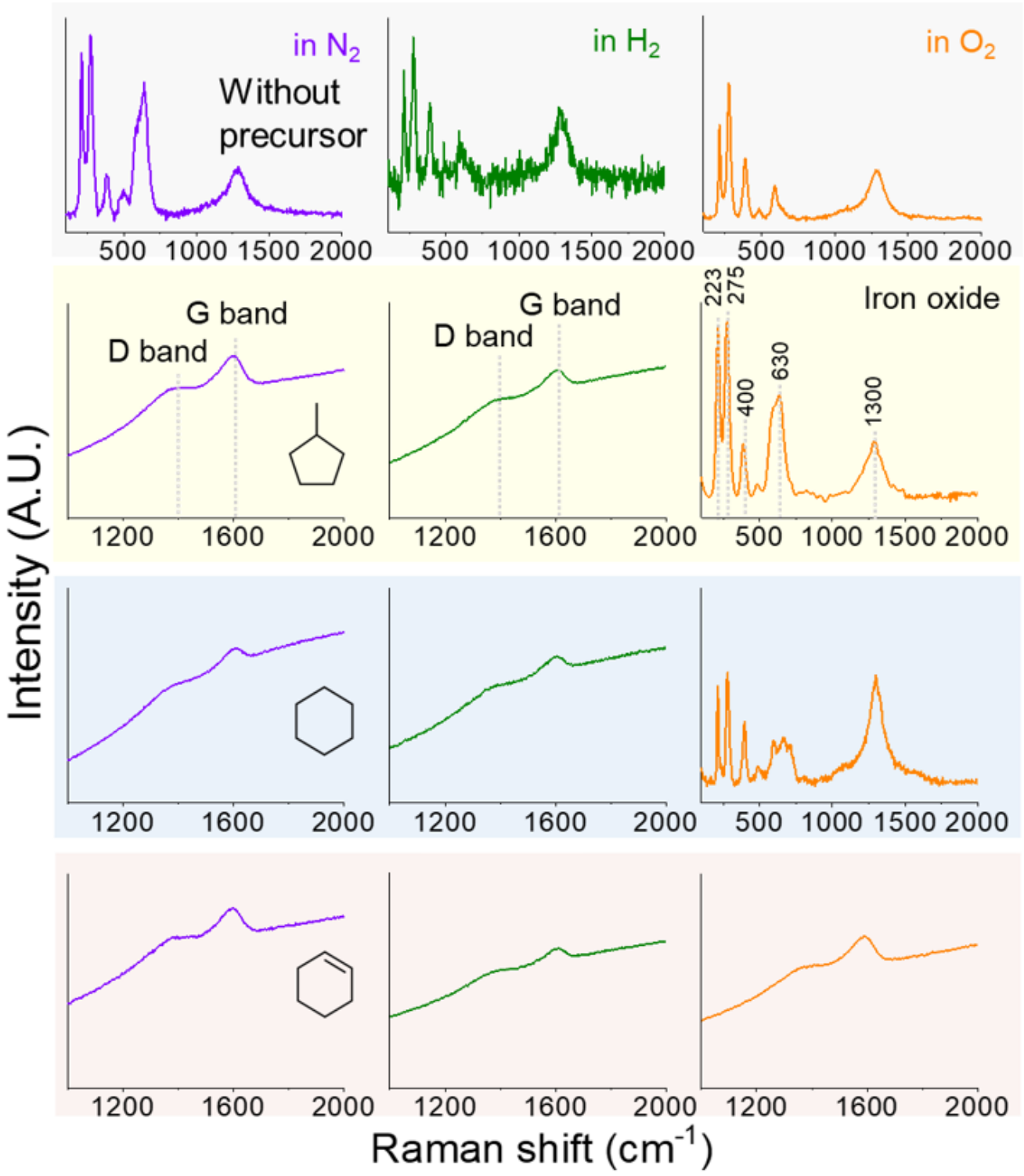

Figure 7

Raman spectra collected at the end of the sliding tracks where tribofilms or wear debris were piled up after 600 reciprocating cycles in 30% P/P_{sat} of precursor vapors in inert (dry N_2), reducing (10% H_2 in N_2), and oxidizing (dry O_2) gas environments. Excitation wavelength = 532 nm; laser power = 2.05 mW; objective lens = 100x (NA = 0.9). The reference spectra of hematite (Fe_2O_3) and magnetite (Fe_3O_4) are shown in Figure S6.

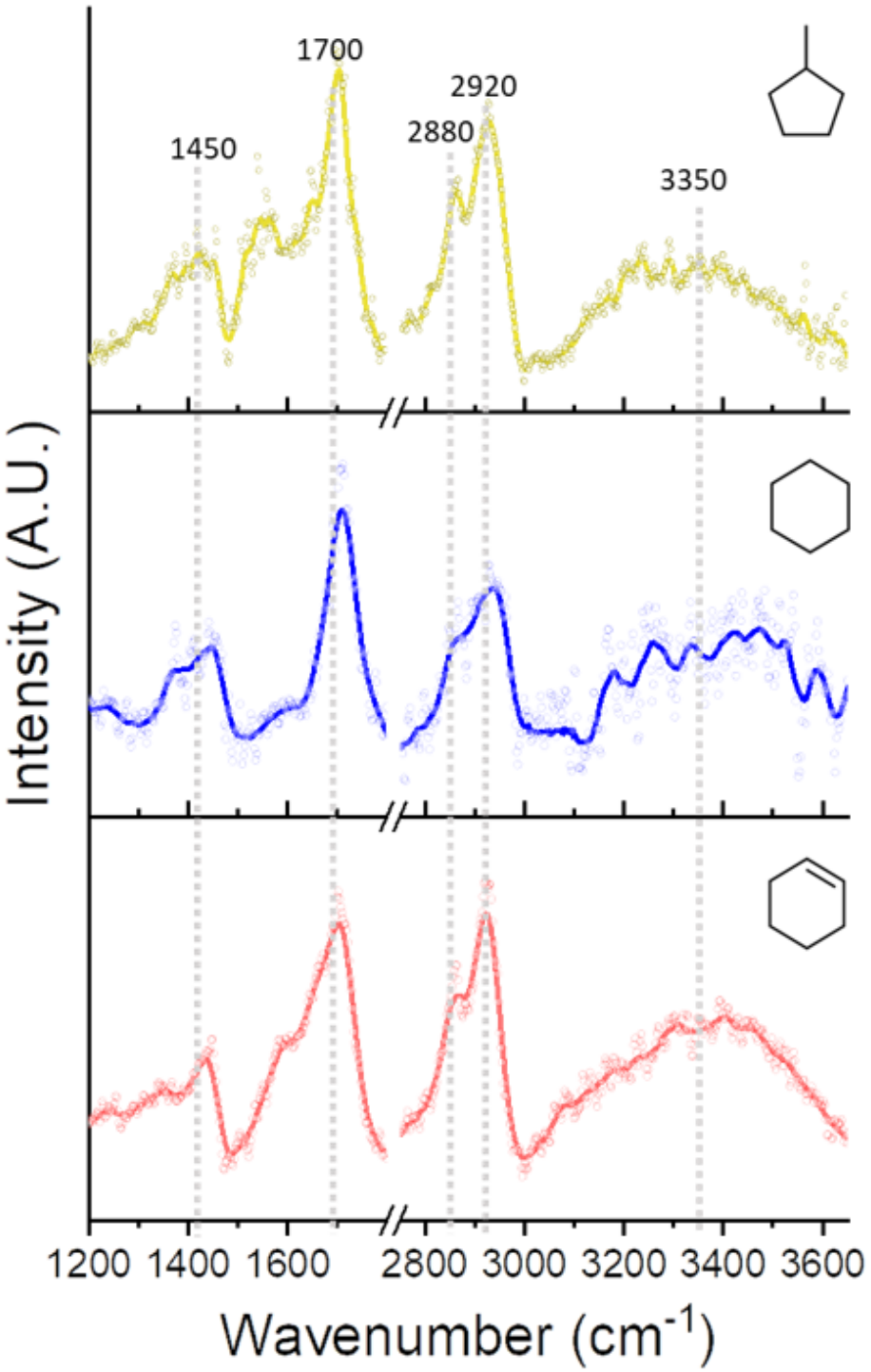

Figure 8

FTIR spectra of triboproducts produced after tribotesting in VPL of methylcyclopentane, cyclohexane and cyclohexene in N_2. Micro-IR objective lens = 15x; analyzed area = 2500 μm^2. (Color figure online)

Supplementary Files

This is a list of supplementary files associated with this preprint. Click to download.

- C6stainlesssteelSIfinal.docx